Earth and Planetary Science Letters 369–370 (2013) 260–270

Contents lists available at SciVerse ScienceDirect

Earth and Planetary Science Letters

journal homepage: www.elsevier.com/locate/epsl

Magnetic signatures of Heinrich-like detrital layers in the Quaternary of the North Atlantic

J.E.T. Channell [a,*], D.A. Hodell [b]

[a] Department of Geological Sciences, POB 112120, University of Florida, Gainesville, FL 32611, USA
[b] Godwin Laboratory for Palaeoclimate Research, Department of Earth Sciences, University of Cambridge, Cambridge CB2 3EQ, UK

ARTICLE INFO

Article history:
Received 23 October 2012
Received in revised form
20 March 2013
Accepted 23 March 2013
Editor: J. Lynch-Stieglitz
Available online 17 April 2013

Keywords:
Heinrich layers
detrital layers
North Atlantic
Quaternary
magnetic properties

ABSTRACT

Magnetic parameters are useful for distinguishing North Atlantic Heinrich-like detrital layers from background sediments. Here we compare magnetic properties with XRF scanning data back to 700 ka and 1.3 Ma at IODP Sites U1302–U1303 and U1308, respectively. Multi-domain magnetite, with grain sizes >20 μm, is characteristic of both Ca- and Si-rich detrital layers, as defined by XRF core scanning, confirming the contribution of ice rafting. Reflectance spectra and magnetic parameters distinguish Ca- and Si-rich IRD layers due the presence of high coercivity hematite in Si-rich layers. Heinrich layer 6 (H6) at Site U1302–U1303 is unlike other detrital layers, being marked by a 45-cm thick homogeneous cream-colored clay layer underlain by a thin (5-cm) graded coarse-sand. Comparison of Site U1302/03 and Site U1308 detrital layers implies a dominant Laurentide source for both Ca- and Si-rich detrital layers. At Site U1308, low benthic $\delta^{13}C$ values during stadials are in-step with magnetic grain-size coarsening associated with Si-rich detrital layers back to 1.3 Ma, indicating a link between deep-sea ventilation and ice rafting. The surface-sediment tan-colored oxic layer ($\sim$2 m thick at Site U1308) yields magnetic hysteresis ratios that are offset from the single-domain to multi-domain (SD–MD) magnetite mixing-line in hysteresis-ratio diagrams. This offset is attributed to maghemite grain-coatings, that form on magnetite in surface sediment, and undergo dissolution as they pass through the oxic/anoxic boundary.

1. Introduction

Heinrich layers in the North Atlantic are cm- to decimeter-scale detrital layers dominated by ice-rafted debris (IRD) deposited by icebergs shed off surrounding continental ice sheets (Heinrich, 1988; Broecker et al., 1992). Heinrich layers deposited in the last 60 kyr have been studied in detail (for review, see Hemming, 2004), and represent a manifestation of the instability of surrounding continental ice-sheets. They provide key information on changes in surface and deep-water conditions associated with these instabilities. They have been correlated to cold stadials in Greenland ice cores and have been implicated in changes in oceanic thermohaline circulation (e.g. Bond et al., 1993, 1999; Bond and Lotti, 1995). For the last glacial cycle, Heinrich layers have been identified in piston cores from throughout the North Atlantic using a combination of high IRD content often comprising detrital carbonate, minima in planktic foraminiferal accumulation rates, and predominance of *N. pachyderma* (sin.) in the foraminiferal assemblage (e.g. Hillaire-Marcel et al., 1994; Van Kreveld et al., 1996; Elliot et al., 1998; Hiscott et al., 2001; Rashid et al., 2003; Rasmussen et al., 2003). Magnetic properties of Heinrich layers include high magnetic susceptibility (e.g., Robinson et al., 1995) and a coarsening of the magnetic grain size parameter, namely the ratio of anhysteretic susceptibility (κ_{ARM}) to susceptibility (κ) (e.g., Stoner et al., 1995, 1996, 1998, 2000).

Integrated Ocean Drilling Program (IODP) Site U1302–U1303 (hereafter referred to as Site U1302/03) and Site U1308 (Fig. 1) collected during IODP Expedition 303 (Channell et al., 2006) have provided records of North Atlantic detrital layers that extend back to 750 ka in the case of Site U1302/03 (Channell et al., 2012) and 1.3 Ma in the case of Site U1308 (Hodell et al., 2008). These two sites provide the most comprehensive record of North Atlantic Heinrich layers, at least prior to the last glacial cycle. Independent age models for the two sites were used to correlate Site U1302/03, from the mouth of the Labrador Sea at Orphan Knoll, to Site U1308 (Fig. 1) in the central Atlantic (Channell et al., 2012). Detrital layers at these two sites have been recognized by a range of parameters: X-ray fluorescence (XRF) core scanning yielding Ca/Sr and Si/Sr ratios indicative of detrital carbonate and detrital silicate minerals, gamma ray attenuation (GRA) density, bulk carbonate $\delta^{18}O$ (Hodell et al., 2008; Channell et al., 2012), and by identification of dolomite using a Fourier Transform Infrared Spectrometer (Ji et al., 2009). At IODP Site U1313, at the southern edge of the North Atlantic IRD belt, Heinrich layers over the last glacial cycle

* Corresponding author. Tel.: +1 352 392 3658; fax: +1 352 392 9294.
E-mail address: jetc@ufl.edu (J.E.T. Channell).

0012-821X/$ - see front matter © 2013 Elsevier B.V. All rights reserved.
http://dx.doi.org/10.1016/j.epsl.2013.03.034

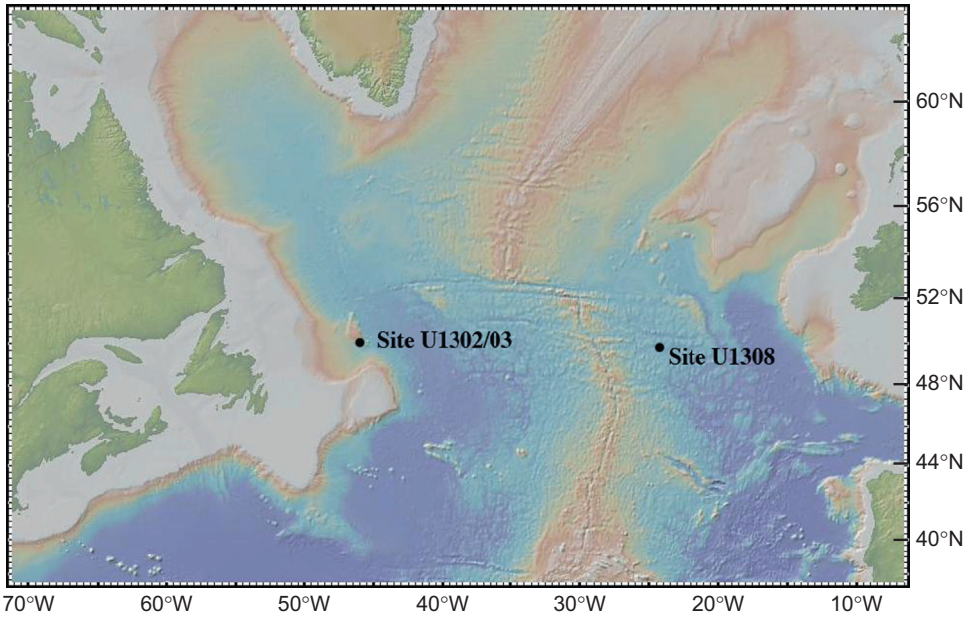

Fig. 1. Location map for IODP Sites U1302–U1303 and U1308.

have been recognized by high quartz/calcite and dolomite/calcite ratios where they are associated with sea surface warming due to northward expansion of the subtropical gyre (Naafs et al., 2013).

At Site U1308, high detrital carbonate (Ca/Sr) layers, labeled "Hudson Strait" Heinrich layers, are associated with peak glacials and glacial terminations back to marine isotope stage (MIS) 16 (Hodell et al., 2008). Site U1302/03, being proximal to Laurentia (Fig. 1), contains many more detrital layers than Site U1308, including additional "Heinrich Strait" Heinrich layers not manifested at Site U1308 (e.g. H0 and H5a). At Site U1302/03, however, Ca-rich and Si-rich detrital layers occur not only in glacial stages but also in most interglacial stages, implying that more than one depositional process (other than IRD deposition) was responsible for detrital layers at Site U1302/03 (Channell et al., 2012). Here we discuss the magnetic signature of Heinrich layers at these two sites in order to elucidate depositional mechanisms and provenance.

2. Methods

The measurement of natural remanent magnetization (NRM), determination of relative paleointensity (RPI) proxies and aspects of the magnetic properties have been reported elsewhere for Site U1302/03 (Channell et al., 2012) and Site U1308 (Channell et al., 2008). Here we are concerned with magnetic properties at these two sites that pertain to magnetic grain size and mineralogy, particularly anhysteretic remanent magnetization (ARM), isothermal remanent magnetization (IRM), magnetic susceptibility and magnetic hysteresis data. The magnetic parameters are compared with previously published Ca/Sr and Si/Sr values obtained from core-scanning XRF and oxygen isotope data, at Site U1308 (Hodell et al., 2008) and Site U1302/03 (Hillaire-Marcel et al., 2011; Channell et al., 2012).

ARM is the laboratory-produced magnetization generated by placing a sample in a strong alternating field (AF), and allowing the peak alternating field to steadily decrease in the presence of a weak uniform DC field. IRM is the laboratory-produced magnetization generated by placing a sample in a strong DC field. ARM and IRM were measured on u-channel samples ($2 \times 2 \times 150$ cm^3 "continuous" samples encased in plastic with a clip-on lid constituting one of the sides) using a 2G Enterprises cryogenic magnetometer at the University of Florida (see Weeks et al., 1993; Guyodo et al., 2002). The ARM was acquired in a peak alternating field of 100 mT and a DC bias field of 50 μT. IRM was acquired using a 2G Enterprises pulse magnetizer built for u-channel samples. ARM was measured at 1-cm spacing prior to demagnetization and then demagnetized at peak alternating fields in the 20–100 mT interval using stepwise 5–10 mT increments (see Channell et al., 2012, 2008). Volume susceptibility was measured at 1-cm intervals on u-channel samples using a susceptibility bridge designed for u-channel samples (Thomas et al., 2003). The response function of the 2G Enterprises u-channel magnetometer is similar to the response function of the susceptibility bridge (see Guyodo et al., 2002; Thomas et al., 2003) thus allowing the calculation of the ratio anhysteretic susceptibility to susceptibility (κ_{ARM}/κ). Anhysteretic susceptibility (κ_{ARM}) is the quantity resulting from dividing (normalizing) ARM intensity by the strength of the DC bias field (50 μT in our case) used in its acquisition. Banerjee et al. (1981) introduced the ratio of anhysteretic susceptibility (κ_{ARM}) to susceptibility (κ) as a monitor of magnetite grain size in sediment cores. The κ_{ARM}/κ ratio depends on empirical observation of a log–log quasi-linear decrease in κ_{ARM} with increasing grain size in the ~0.05–100 μm grain size range (e.g., Egli and Lowrie, 2002). Although mass susceptibility tends to increase with grain size in the 1–100 μm range, it is relatively independent of grain size compared to κ_{ARM}, so that κ serves to normalize κ_{ARM} for changes in magnetite concentration. A caveat is that ultrafine (superparamagnetic) magnetite grains (< 0.03 μm) can have relatively high mass susceptibility leading to κ_{ARM}/κ values that mimic coarse (multidomain) grains. The κ_{ARM}/κ ratio has been empirically calibrated for the 0.1–200 μm grain size range (Dankers, 1978; Banerjee et al., 1981; King et al., 1983), and we use this calibration to assess magnetite (magnetic) grain size within detrital layers and in intervening background sediments.

The S-ratio is a parameter sensitive to coercivity, the "hardness" of the magnetization in AF demagnetizing fields, and can be characteristic of magnetic mineralogy. The S-ratio can be calculated as the ratio of the IRM acquired in a DC back-field of 0.3 T, divided by an initial IRM acquired in a DC forward-field of 1 T (King and Channell, 1991). Because the coercivities for magnetite lie almost entirely below 0.3 T, irrespective of grain-size or composition, and hematite coercivities would be expected to be

above 0.3 T, the S-ratio is useful for detecting the presence of hematite in marine sediments. Variations in sediment redness are expressed in shipboard color reflectance data as a*, red–green reflectance (Expedition 303 Scientists, 2006). The primary mineral imparting the red color to sediment is often hematite, which is marked by a diagnostic peak in the first derivative of reflectance in the 555–575 nm wavelength range (Barranco et al., 1989; Deaton and Balsam, 1991). We use the S-ratio, and the difference in reflectance for wavelengths of 560 and 570 nm, as monitors for hematite at Site U1302/03 and Site U1308, respectively.

Day et al. (1977) introduced the so-called "Day" plot of the ratio of saturation remanence (M_r) to saturation magnetization (M_s) versus the ratio of remanent coercivity (H_{cr}) to coercive force (H_c) for assessing titanomagnetite grain size and domain state. These authors discriminated fields corresponding to single domain (SD) and multidomain (MD) grains, with a broad transitional field corresponding to pseudo-single domain (PSD) grains, that are theoretically large enough to be MD, but are magnetically more similar to SD grains, probably due to discontinuities and dislocations characteristic of natural (detrital) magnetite. Alternatively, the PSD field in a Day plot may represent a zone of mixing of SD and MD magnetite grains. Deep-sea (pelagic) sediments usually contain detrital titanomagnetite, and hysteresis ratios usually lie in the PSD field of a Day plot (e.g. Channell et al., 2008). Empirical and theoretical calibrations of the Day plot (Day et al., 1977; Carter-Stiglitz et al., 2001; Dunlop, 2002a, 2002b; Dunlop and Carter-Stiglitz, 2006) can be utilized to assign "mean" magnetite grain sizes to hysteresis ratios. At Site U1302/03 and Site U1308, small (few hundred mg) samples were collected at regular intervals (every few cm) using a toothpick, inserted in a #4 gel-cap and then attached to the probe of a Princeton Measurements Corp. vibrating sample magnetometer (VSM). Backfield measurements were used to estimate H_{cr}, and hysteresis loop measurements carried out in a maximum applied field of 1 T provided values of H_c, M_r and M_s. Magnetic hysteresis properties were also analyzed through so-called First-Order Reversal Curves (FORCs) that provide enhanced mineral and domain state discrimination (Pike et al., 1999; Roberts et al., 2000; Muxworthy and Roberts, 2007). The FORCs were measured on the VSM, and carried out by progressively saturating a small (few hundred mg) sample in a field (H_{sat}), decreasing the field to a value H_a, reversing the field and sweeping it back to H_{sat} in a series of regular field steps (H_b). The process is repeated for many values of H_a. The magnetization is then represented as a contour plot with axes B_c and B_u where $B_c=(H_b-H_a)/2$ and $B_u=(H_b+H_a)/2$. The contoured distribution of a FORC can be interpreted in terms of the coercivity distribution

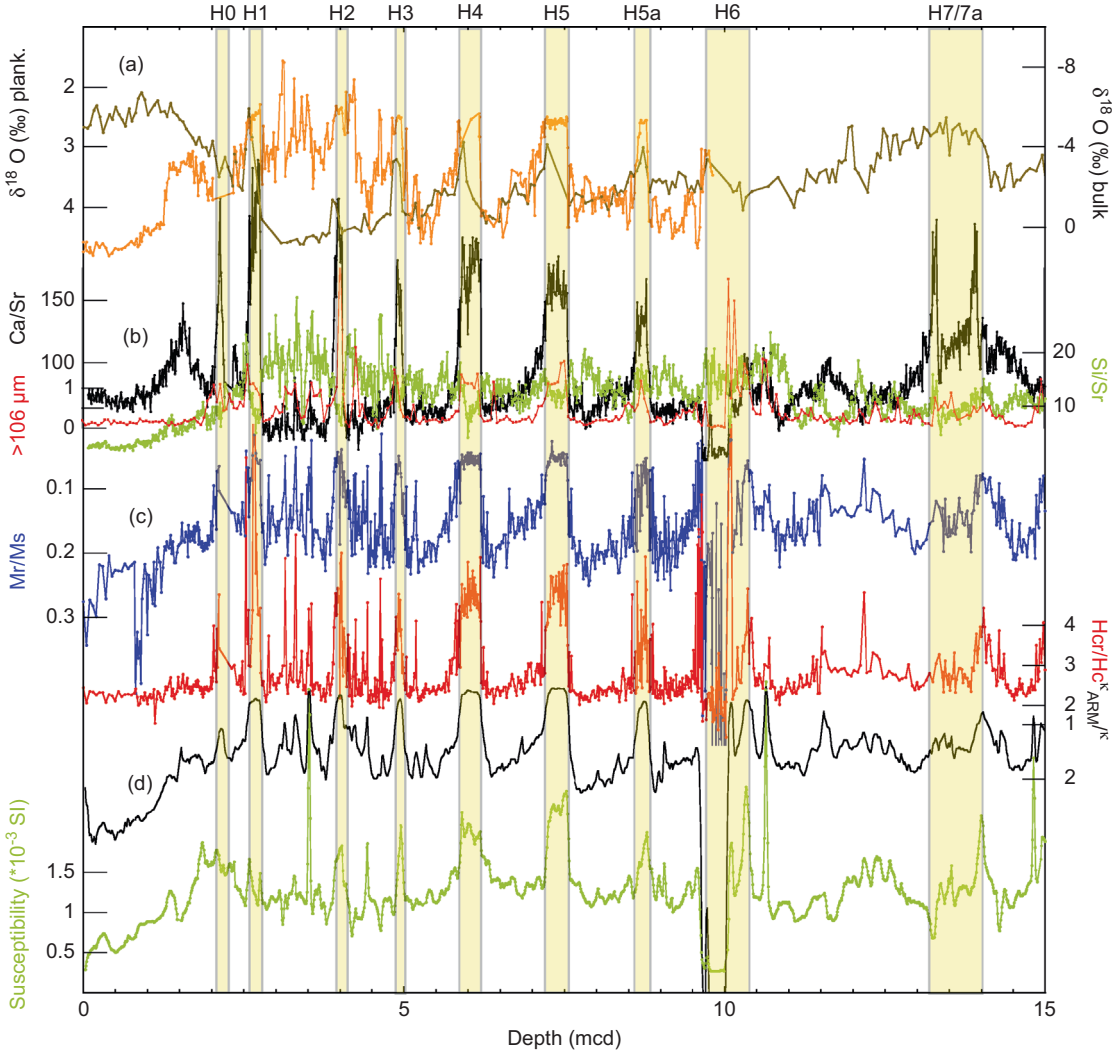

Fig. 2. IODP Site U1302–U1303, for 0–15 m composite depth (mcd): (a) brown, planktic $\delta^{18}O$ (Hillaire-Marcel et al., 2011); orange, bulk carbonate $\delta^{18}O$. (b) Black, Ca/Sr counts from XRF core scanning; light green, Si/Sr counts from XRF core scanning (Channell et al., 2012); red, > 106 µm %wt (Hillaire-Marcel et al., 2011). (c) Blue, hysteresis ratio M_r/M_s; red, hysteresis ratio H_{cr}/H_c. (d) Black: κ_{ARM}/κ, magnetite grain size proxy; green: volume susceptibility. Shaded intervals are associated with Heinrich Events (H0–H7). (For interpretation of the references to color in this figure legend, the reader is referred to the web version of this article.)

along the B_c axis. Spreading of the distribution along the B_u axis corresponds to magnetostatic interactions for SD grains or internal demagnetizing fields for MD grains, although the latter dominates in weakly magnetized deep-sea sediments, and spreading in B_u combined with low B_c can be interpreted in terms of high MD titanomagnetite content. In general, closed peaked structures along the B_c axis are characteristic of SD grains, with contours becoming progressively more parallel to the B_u axis with grain-size coarsening. FORC diagrams were analyzed using the software of Harrison and Feinberg (2008) with smoothing factors (SF) of 6. The relatively high smoothing factor is necessary to suppress noise for weakly magnetized bulk sediments, in spite of a FORC protocol lasting 3.6 hours with an averaging time of 1 s and a field increment of 2 mT up to a maximum applied field of 1 T.

Finally, IRM acquisition curves for a few bulk sediment samples placed in #4 gel-caps were generated using the VSM. The IRM was measured at one hundred magnetizing field steps, interpolated to be uniformly spaced on a logarithmic scale from ~7 mT to 1 T. The IRM acquisition curves were then analyzed for coercivity components using IRM-UNMIXER software (see Heslop et al., 2000) that relies on the supposition of Robertson and France (1994) that, in the absence of magnetic interactions, the first derivatives of IRM acquisition curves yield log-normal probability density functions that represent coercivity spectra.

3. Detrital layer stratigraphy

Age models for Sites U1302–1303 were based on planktic oxygen isotopes and relative paleointensity data (Hillaire-Marcel et al., 2011; Channell et al., 2012) and for Site U1308 on benthic oxygen isotope data (Hodell et al., 2008). The age models for these two sites have been used to demonstrate apparent synchronicity of certain detrital layers between the two sites (Channell et al., 2012). In this paper, we compare magnetic methods for determining magnetic grain size and mineralogy, and demonstrate the usefulness of magnetic data for recognizing detrital layers and constraining mode of deposition and provenance.

Parameters sensitive to magnetic grain size (κ_{ARM}/κ, M_r/M_s and H_{cr}/H_c) and magnetic mineralogy (S-ratio) are compared to susceptibility (a magnetic concentration parameter), reflectance data (labeled 560–570 nm) and XRF scanning data (Ca/Sr and Si/Sr) for Site U1302/03 (Figs. 2 and 3) and Site U1308 (Fig. 4). The 0–15 m composite depth (mcd) interval at Site U1302/03 records H0–H7 (Fig. 2). All labeled detrital layers in this interval, other than H6, are characterized by high Ca/Sr ratios indicating high detrital carbonate content. Peaks in Ca/Sr are accompanied by increased magnetic grain size, as indicated by κ_{ARM}/κ, M_r/M_s and H_{cr}/H_c (Fig. 2), and usually by susceptibility peaks indicating high magnetite concentration. The Ca/Sr peak for H7a, but not that

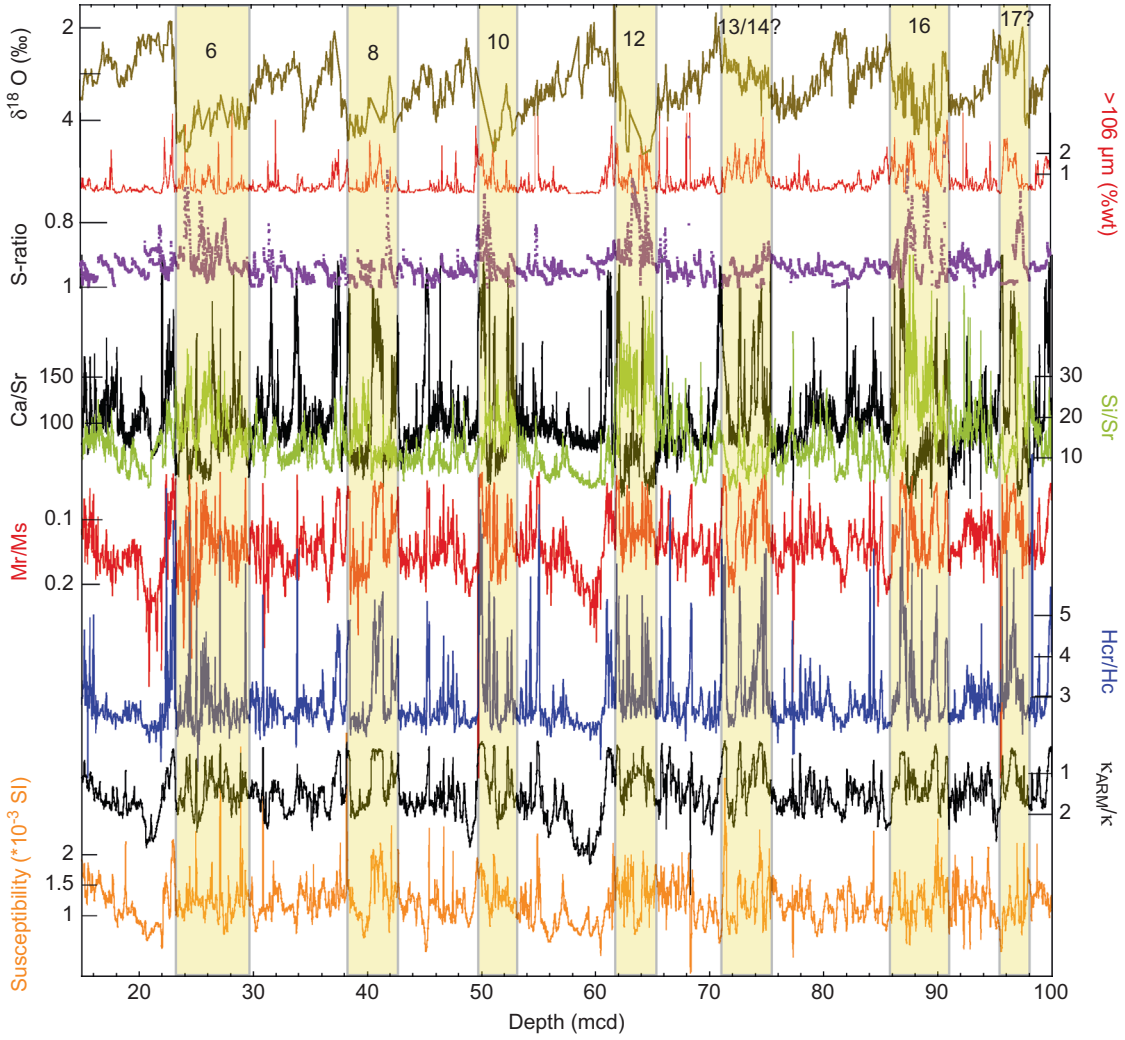

Fig. 3. IODP Site U1302–U1303, for 15–100 m composite depth (mcd). From top: planktic $\delta^{18}O$ (brown) and >106 µm %wt (red) (Hillaire-Marcel et al., 2011); S-ratios (purple); Ca/Sr (black) and Si/Sr (green) from XRF core scanning (Channell et al., 2012); hysteresis ratios M_r/M_s (red) and H_{cr}/H_c (blue); κ_{ARM}/κ magnetite grain size proxy (black); and volume susceptibility (orange). Shaded intervals mark marine isotope stages (numbered). High levels of IRD are represented by XRF ratios (Ca/Sr and Si/Sr), wt% >106 µm, S-ratios and magnetic grain-size parameters. (For interpretation of the references to color in this figure legend, the reader is referred to the web version of this article.)

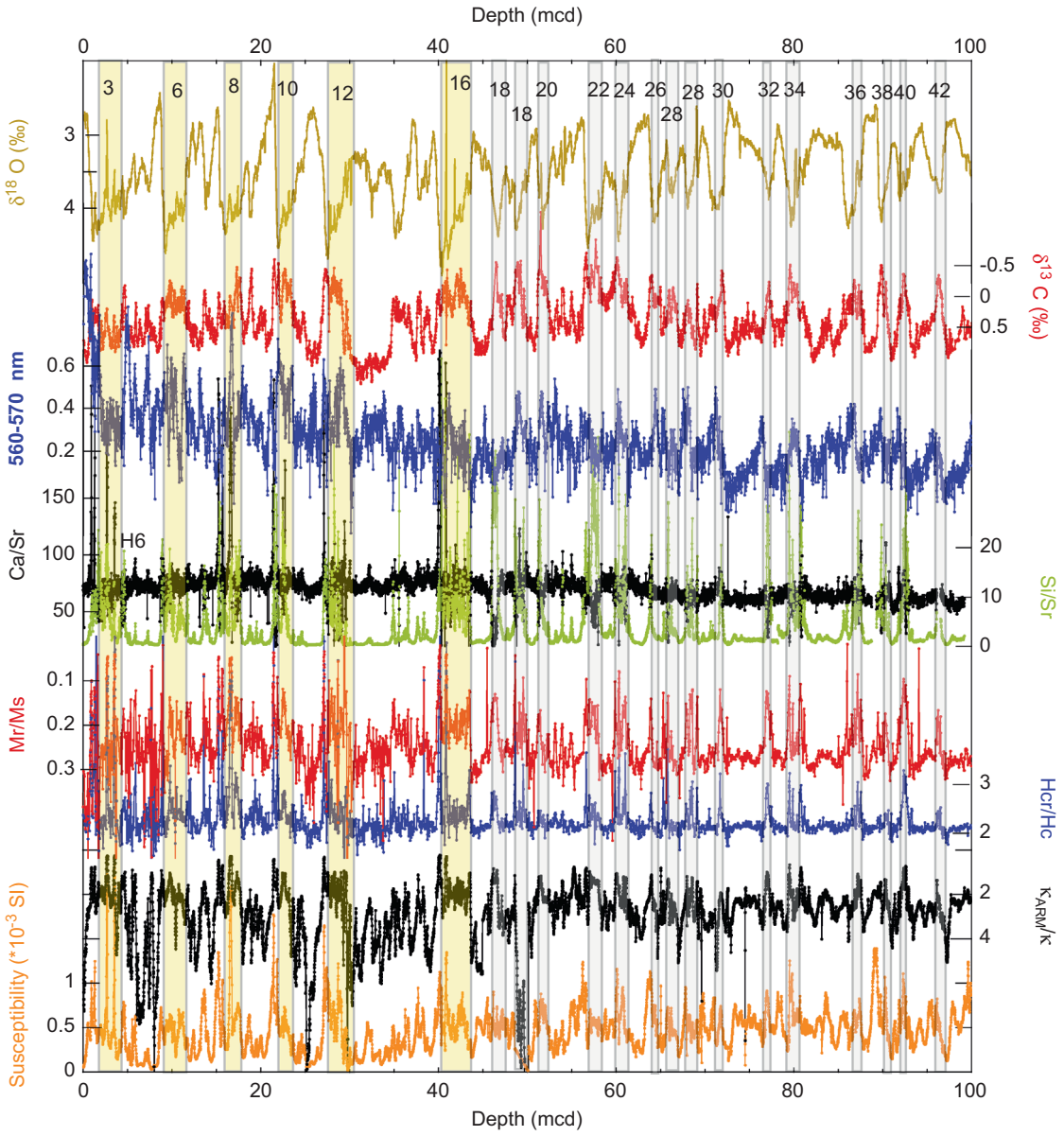

Fig. 4. IODP Site U1308, for 0–100 m composite depth (mcd). From top: benthic $\delta^{18}O$ (brown) and $\delta^{13}C$ (red); change in reflectance in the 560–570 nm wavelength band (blue); Ca/Sr counts (black) and Si/Sr (green) from XRF core scanning (Hodell et al., 2008); hysteresis ratios M_r/M_s (red) and H_{cr}/H_c (blue); κ_{ARM}/κ, magnetite grain size proxy (black) and volume susceptibility (orange). Glacial marine isotopic stages are shaded and numbered back to MIS 42. (For interpretation of the references to color in this figure legend, the reader is referred to the web version of this article.)

for H7, is manifest in susceptibility and in magnetic grain-size parameters. In many cases, magnetic grain-size parameters indicate detrital layers characterized by sharp bases and (bioturbated) gradational tops. Three low detrital carbonate (LDC) events are observed between H1 and H2 (see Stoner et al., 1998) that are characterized by high Si/Sr ratios, coarse magnetic grain size, with the oldest of the three LDC events being associated with high susceptibility (Fig. 2). At least one, possibly two, LDC event (s) occur between H2 and H3. These LDC events are particularly well marked by hysteresis ratios (M_r/M_s and H_{cr}/H_c). Estimated ages for H0–H6 at Site U1302/03 are given in Table 1 of Channell et al. (2012). H7 and H7a at Site U1302/03 lie in the 85–90 ka interval, within MIS 5b.

H6 at Site U1302/03 has different characteristics from the younger Heinrich events. It lacks a prominent Ca/Sr or Si/Sr peak, but is manifest by a ~45-cm-thick cream-colored homogeneous clay layer (95% clay) that is devoid of carbonate (low Ca/Sr) and characterized by ultra-fine (submicron) magnetite grain-size, low susceptibility, low density, and negligible IRD (wt% >106 μm) (Figs. 2 and 5). The clay layer is underlain by 5-cm-thick graded interval from very-coarse sand to medium sand, and then a sharp contact with the overlying clay (Fig. 5). Silty-clays with elevated Ca/Sr and wt% >106 μm grain-size lie immediately below the graded sand layer, and silty-clays with slightly elevated Si/Sr lie immediately above the clay layer (Figs. 2 and 5).

In the 15–100 mcd interval at Site U1302/03, comprising most of the Brunhes Chronozone back to ~700 ka, detrital layers are marked by Ca/Sr and Si/Sr peaks, and by increased magnetite grain-size from κ_{ARM}/κ, M_r/M_s and H_{cr}/H_c (Fig. 3). Detrital layers denoted by XRF ratios and higher magnetic grain-size occur in all glacial and interglacial stages, with the exception of MIS 11. Elevated Si/Sr is observed in glacial intervals (particularly MIS 6, 12, 16) and are associated with elevated magnetic grain size, high >106 μm wt%, and low S-ratios, implying the presence of a high-coercivity mineral such as hematite (Fig. 3). High Si/Sr intervals can be associated with increased silicate-rich IRD, rather than reduced carbonate content, because magnetic

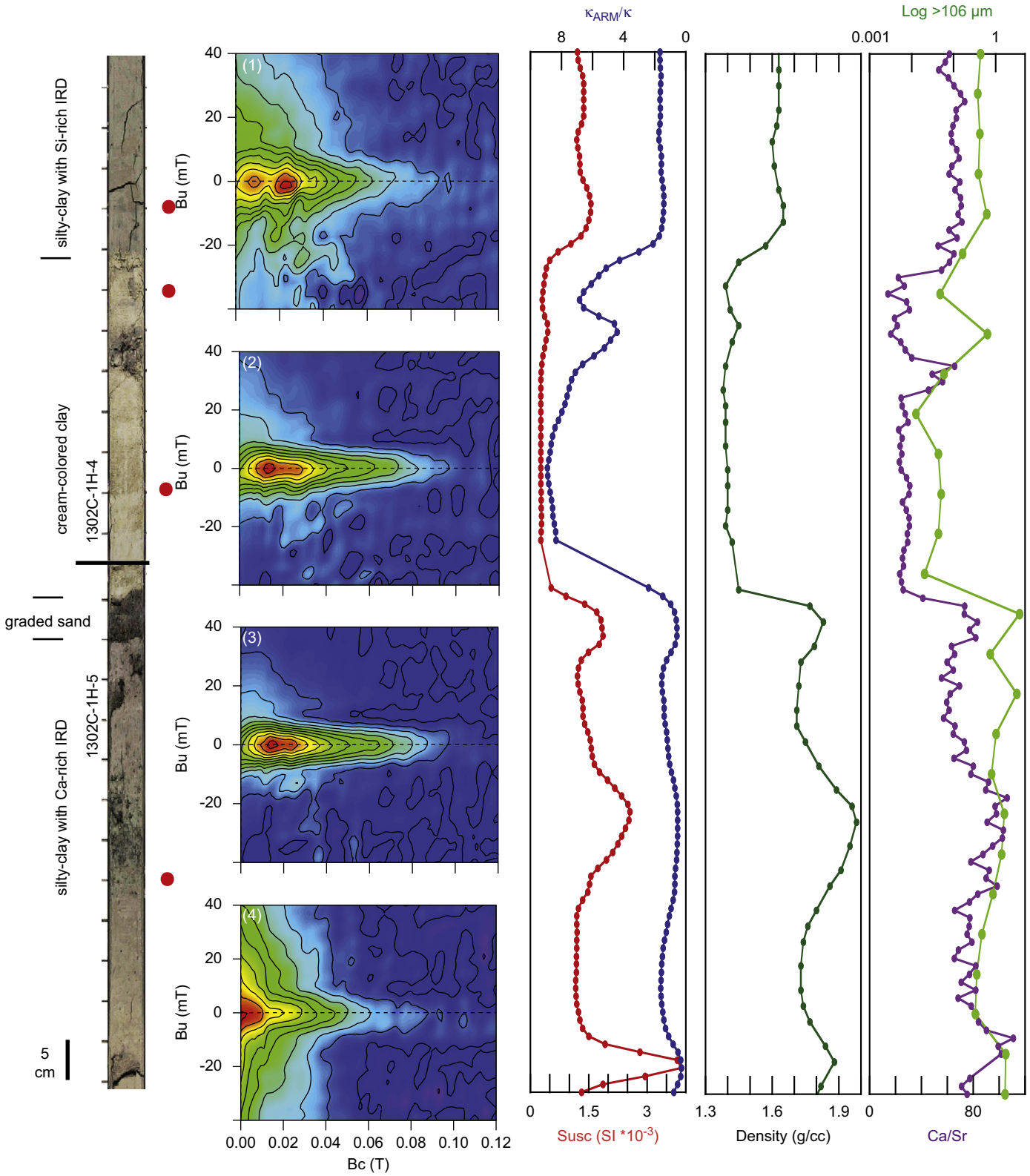

Fig. 5. Heinrich Layer 6 (H6) recorded at IODP Hole 1302C. First-order reversal curves (FORCs) are from samples at locations marked by red circles adjacent to core photographs. A cream-colored clay layer (devoid of carbonate) overlies a 5-cm graded sand layer. Silty clays above and below contain ice-rafted debris (IRD). The cream colored clay layer is marked by fine magnetite grain size (high κ_{ARM}/κ), low susceptibility, low density, and low values of Ca/Sr (and Si/Sr). FORCs from FORCinel software of Harrison and Feinberg (2008) using a smoothing factor of 6. (For interpretation of the references to color in this figure legend, the reader is referred to the web version of this article.)

grain-size parameters are independent of concentration variations that would result from carbonate dilution.

At Site U1308, prominent Ca/Sr anomalies are observed in glacial stages back to MIS 16 (Hodell et al., 2008) (Fig. 4). Si/Sr anomalies are observed in glacial stages MIS 8, 10, 12 and 16, and in glacial stages prior to MIS 16. Hodell et al. (2008) observed the association of Si/Sr peaks with low values of benthic $\delta^{13}C$ implying a link between iceberg discharge, lowered salinity and weakening

thermohaline circulation. Magnetic grain size parameters (κ_{ARM}/κ, M_r/M_s and H_{cr}/H_c) at Site U1308 indicate that high Si/Sr and low benthic $\delta^{13}C$ values are associated with grain size coarsening implying enhanced silicate IRD input and deep-water circulation changes during glacial intervals back to MIS 42 (~1.3 Ma). The change in 560–570 nm reflectance co-varies with magnetic grain-size coarsening indicating that silicate-rich detrital layers have higher hematite content than background sediments and carbonate-rich detrital layers. Carbonate-rich detrital layers are associated with strong susceptibility peaks whereas susceptibility peaks for silicate-rich detrital layers are muted (Fig. 4).

Plots of anhysteretic susceptibility (κ_{ARM}) versus susceptibility (κ) are expected to be quasi-linear for uniform magnetite grain size with magnetite concentration increasing with distance from the origin (Fig. 6). The calibration of this plot in terms of (magnetite) grain-size is empirical, and stems from the work of King et al. (1983). Magnetic concentration (note scale differences in Fig. 6) and magnetic grain size are greater for Site U1302/03 than for Site U1308. Magnetite grain size apparently varies in the submicron to 25 μm range at both sites (Fig. 6).

Hysteresis ratios from Sites U1302/03 and U1308 usually lie along the well-known SD–MD mixing line for magnetite on Day plots (Fig. 7). A theoretically and empirically calibrated SD–MD mixing line for titanomagnetite (Carter-Stiglitz et al., 2001; Dunlop, 2002a, 2002b; Dunlop and Carter-Stiglitz, 2006) is shown by light green triangles in Fig. 7a–c, and empirical data for sized (unannealed) natural magnetite (Dunlop et al., 2002a) are shown in Fig. 7a. At Site U1302/03, background sediments plot in the PSD field (Fig. 7b) and those from Site U1308 plot also in the PSD field but in the finer-grained segment of the magnetite mixing line (Fig. 7c). Background sediments appear to have "average" magnetite grain-size in the ~0.5–4 μm range at Site U1308 and 0.8–10 μm at Site U1302/03, broadly consistent with the κ_{ARM}/κ distributions (Fig. 6). Hysteresis ratios associated with detrital layers extend into the MD field, beyond 20 μm, for both Ca-rich and Si-rich detrital layers at both sites (Fig. 7b and c). The merging of data points from detrital layers and background sediments along the magnetite mixing line is partly attributable to bioturbation of Heinrich layers and background sediments, particularly close to the top of detrital layers.

At Site U1308, hysteresis data associated with H1 and H2, and associated background sediment, lie off the SD–MD magnetite mixing line (open symbols in Fig. 7c). This is attributed to the occurrence of H1 and H2 at Site U1308 within the oxic (ochre-colored) surface sediment layer, which is ~2 m thick at this site but only about 10 cm thick at Site U1302/03. The difference in thickness of the oxic surface-sediment layer is attributed to lower sedimentation rate and lower level of organic-matter burial at Site U1308 with respect to Site U1302/03. The shift of the oxic surface sediment layer from the SD–MD mixing line is due to the high values of H_{cr} in the oxic zone (~60 mT compared to ~30 mT below the oxic zone), and can be attributed to maghemite rims forming on titanomagnetite in the surface layer that undergo dissolution as the sediment is buried below the oxic zone. Smirnov and Tarduno (2000) have given a similar explanation for offset of hysteresis ratios from the magnetite mixing line for surface sediment from the western equatorial Pacific.

FORC diagrams allow discrimination of detrital carbonate layers, detrital silicate layers, and background sediment, and perhaps for sediments from the oxic surface sediment layer at Site U1308 (Fig. 8). FORC diagrams on the left side of Fig. 8 represent FORCs from high Ca/Sr detrital layers: H1 (Hole 1303B, Fig. 8A), H2 (Hole 1303B, Fig. 8B) and for high Ca/Sr values within MIS 8 (Holes 1302A/1308E, Fig. 8C and D). The center column of Fig. 8 represents FORC diagrams from background sediment immediately below H1 at Hole 1303B (Fig. 8E), below H2 at Hole 1303B (Fig. 8F), in MIS 8 at Hole 1302A (Fig. 8G) and MIS 17 at Hole 1308A (Fig. 8H). Fig. 8I depicts H1 from Hole 1308C within the oxic zone indicating a higher coercivity "tail" to the FORC diagrams that we attribute to maghemite coatings on magnetite grains. The rest of the right-side column of Fig. 8 represents silicate-rich detrital layers from Holes 1302C and 1308A (Fig. 8J and K) and Hole 1308A (Fig. 8L). The carbonate-rich detrital layers have FORC diagrams (Fig. 8A–D) indicating coarse MD magnetite showing low coercivity, and spreading along the B_u axis due to internal demagnetizing fields. These samples plot either within or close to the MD field in the Day plots (Fig. 7a), and have the lowest slopes in the κ_{ARM} versus κ plots (Fig. 6). The silicate-rich (high Si/Sr) detrital layers also appear to have characteristic FORC diagrams (Fig. 8J–L) with the ridge along the B_c axis being associated with higher coercivities and with spreading along the B_u axis. Background sediments (center column in Fig. 8) show reduced spreading along B_u and similar coercivity distribution to the silicate-rich detrital layers. One sample from immediately below H1 (Fig. 8E) is transitional between carbonate-rich detrital layers and background sediment.

The first derivative of IRM acquisition curves can be modeled in terms of magnetic coercivity spectra (see Kruiver et al., 2001; Heslop et al., 2000). For background sediments and Ca-rich (high Ca/Sr) detrital layers, adequate fit can be achieved using two log-normal coercivity spectra, a prominent one centered on an applied

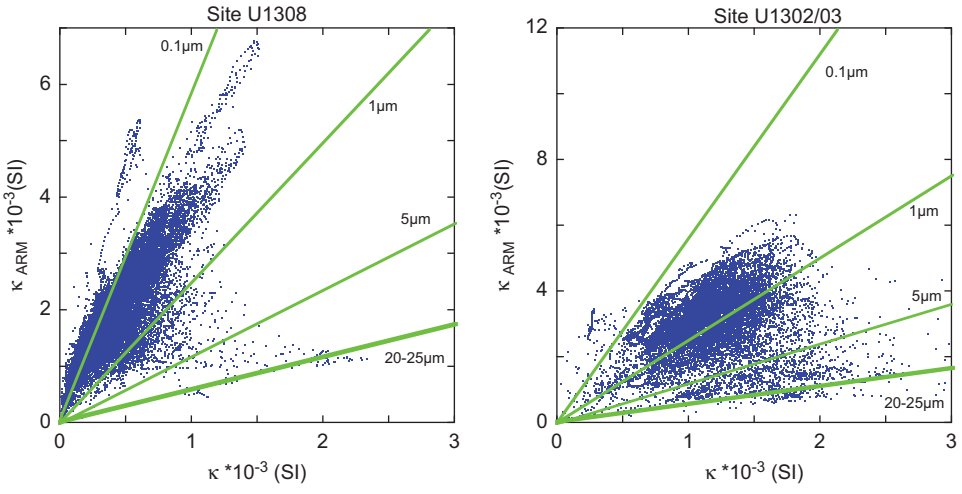

Fig. 6. Sites U1308 and U1302/03: anhysteretic susceptibility (κ_{ARM}) versus volume susceptibility (κ) for 20 mT peak demagnetization field applied to the anhysteretic remanence (ARM) with magnetite grain-size calibration from King et al. (1983).

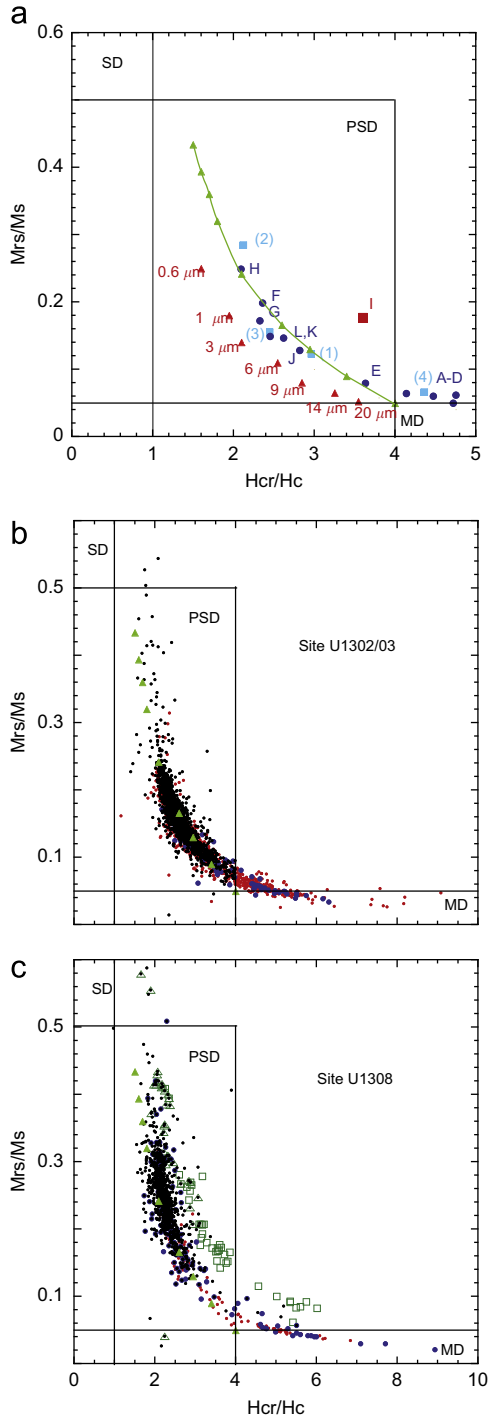

Fig. 7. Hysteresis ratio plots after Day et al. (1977) for IODP Sites U1302–U1303 and U1308, indicating fields for single-domain (SD), pseudo-single domain (PSD) and multidomain (MD) magnetite. (a) Dark blue circles represent hysteresis ratios for FORC data in Fig. 8 labeled A–L. Light blue squares show hysteresis ratios for FORC data in in Fig. 5 labeled (1)–(4). Red square represents hysteresis ratios for FORC in Fig. 8I (from the upper oxic zone of Site U1308). Red triangles: sized natural magnetites (unannealed) from Dunlop (2002a). Closed light green triangles: SD (100%)–MD (100%) magnetite mixing models based on linear mixing model and mixing from hysteresis loops (Carter-Stiglitz et al., 2001; Dunlop and Carter-Stiglitz, 2006; Dunlop, 2002a). (b) IODP Site U1302–U1303. Black dots: background sediments. Solid red circles: data from Ca-rich detrital layers. Solid blue circles from Si-rich detrital layers (MIS 12 and 16). Closed light green triangles as for Fig. 7a. (c) IODP Site U1308. Black dots: background sediment with open green triangles for background sediment from the uppermost oxic zone. Open green squares: H1 and H2 (from oxic zone). Solid red circles: data from Ca-rich detrital layers. Solid blue circles: data from Si-rich detrital layers (MIS 12 and 16). Closed light green triangles as for Fig. 7a. (For interpretation of the references to color in this figure legend, the reader is referred to the web version of this article.)

field of ~50–60 mT and a broader spectrum centered on a lower field in the 15–40 mT range that may be associated with the coarser IRD component (Fig. 9a–d). Increased asymmetry in the first-derivative (gradient) curve is apparent for detrital layers relative to background sediments (compare Fig. 9a and b). In the case of Si-rich detrital layers (Fig. 9e and f), the gradient curves cannot be adequately matched using two coercivity spectra, but require a third coercivity spectrum for which saturation is not achieved in the maximum applied field (1T). We associate this unsaturated high-coercivity component in Si-rich detrital layers with hematite, also detected by 570–560 nm reflectance and S-ratios. The hematite component is not apparent in hysteresis loops (they are not wasp-waisted), but is apparent in FORC diagrams (Fig. 8) carried out on the same samples used for IRM acquisition (Fig. 9).

4. Conclusions

Magnetite, or titanomagnetite, is the dominant magnetic mineral in pelagic sediments in general, as well as in Quaternary pelagic sediments of the North Atlantic. The sensitivity of magnetic grain-size estimates for magnetite lies in the transitional behavior of the magnetic characteristics of this mineral as grain size changes from SD (single domain) to MD (multi-domain). Magnetic parameters are sensitive to grain sizes in the 0.03 μm to several tens of μm range for magnetite, a grain size range that is largely below the reach of physical grain size determinations using Sedigraph or laser-based methods, but in the grain-size range that dominates detritus in the pelagic realm. Magnetic grain-size proxies such as κ_{ARM}/κ and magnetic hysteresis parameters (M_r/M_s and H_{cr}/H_c) are useful for detecting North Atlantic Heinrich-like layers. These grain size parameters can be rapidly acquired and augment detection methods based on physical properties (e.g. density and reflectance), bulk $\delta^{18}O$ (Hodell and Curtis, 2008), and XRF scanning for elemental ratios such as Ca/Sr and Si/Sr (Hodell et al., 2008).

Magnetic grain size parameters have been empirically and theoretically calibrated for magnetite, allowing estimates of magnetic grain sizes for detrital layers and background pelagic sediment. Detrital layers and background sediment at IODP Sites U1302/03 and U1308 lie on the SD–MD mixing line for magnetite on the Day et al. (1977) hysteresis ratio plot. At both sites, Ca-rich and Si-rich detrital layers, marked by high Ca/Sr and Si/Sr ratios, reach into the MD field of the Day plot indicating grain sizes in excess of ~20 μm (Fig. 7). The estimate is broadly compatible with maximum grain size estimates from the κ_{ARM} versus κ plot (Fig. 6). We expect magnetic grain size estimates to represent minimum estimates of average sediment grain size due to the high density of magnetite (5.18 g/cm^3) relative to other sedimentary constituents, and the fact that magnetite may occur as inclusions in larger detrital grains. IRM acquisition curves can be modeled by two distinct coercivity populations for Ca-rich detrital layers, indicating a mixture of magnetite from IRD and background deposition, and, in the case of Si-rich detrital layers, a third high-coercivity (hematite) component (Fig. 9).

H6 is unlike other Heinrich layers within the last glacial at Site U1302/03, or older detrital layers at either site (Fig. 2). At Site U1308, H6 coincides with a broad Si/Sr anomaly (see Fig. 5 of Hodell et al., 2008, or Fig. 5 of Channell et al., 2012), no Ca/Sr peak, and muted magnetic grain size coarsening and susceptibility peaks. At Site U1302/03, H6 is manifest by a 45-cm-thick cream-colored clay layer devoid of carbonate that is underlain by a thin (5-cm) graded sand layer (Fig. 5). Below the graded bed, silty clays contain Ca-rich IRD as indicated by the wt% > 106 μm, Ca/Sr and magnetic grain size parameters (Figs. 2 and 5). Si-rich IRD appear

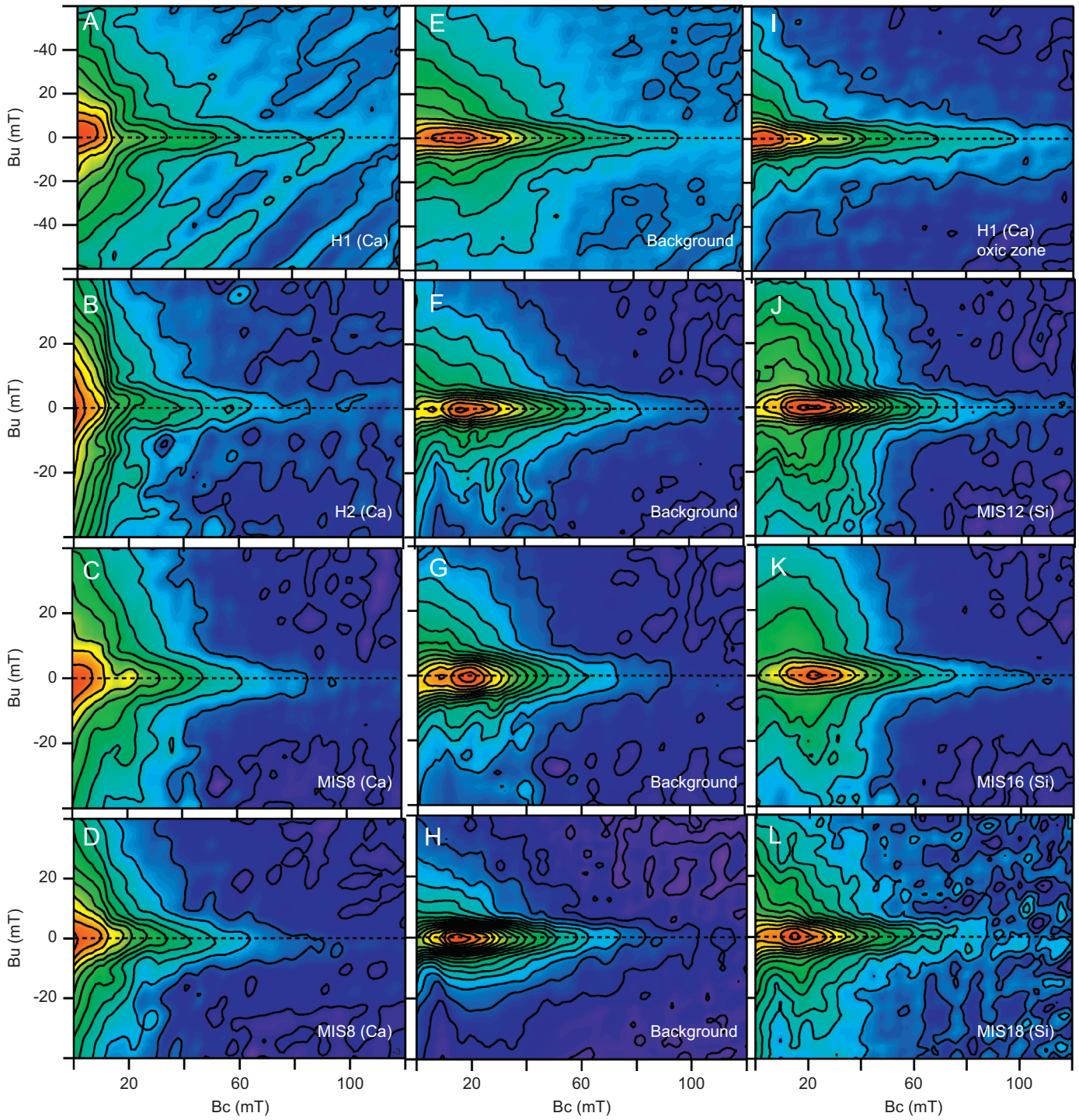

Fig. 8. IODP Sites U1302–U1303 and U1308: First Order Reversal Curves (FORCs) for carbonate-rich detrital layers (A–D), background sediment (E–H), carbonate-rich detrital layer from surface oxic layer (I), and silicate-rich detrital layers (J–L). (A) 1303B-1H-2, 43 cm (H1), (B) 1303B-1H-3, 17 cm (H2), (C) 1302 A-4H-4, 40 cm (39.38 mcd, MIS 8), (D) 1308E-2H-2, 135 cm (15.65 mcd, MIS8), (E) 1303B-1H-2, 45 cm (2.77 mcd, 2-cm below A), (F) 1303B-1H-3, 130 cm (5.12 mcd, MIS 3), (G) 1302 A-4H-4, 5 cm (39.38 mcd, MIS 8), (H) 1308 A-5H-3, 5 cm (44.97 mcd, MIS 17), (I) 1308C-1 H-1, 84 cm (0.84 mcd, H1 from the surface oxic layer), (J) 1302C-7 H-1, 30 cm (63.43 mcd, MIS 12), (K) 1302 A-9 H-4, 5 cm (88.96 mcd, MIS 16), (L) 1308 A-5 H-3, 75 cm (45.66 mcd, MIS 18). FORCs derived using FORCinel software of Harrison and Feinberg (2008) using a smoothing factor of 6.

to be present immediately above the clay layer as indicated by Si/Sr and magnetic grain size parameters. The clay layer and the underlying graded interval may be attributed to massive turbidites funneled down the nearby North Atlantic Mid-Ocean Channel (NAMOC), with the 45-cm clay layer having been deposited at Site U1302/03 from large volumes of clay-sized sediment lofted into suspension by turbiditic activity.

The surface sediment oxic layer at Site U1308 is ~2 m thick in contrast to a thin ~10 cm oxic layer at Site U1302/03, the difference being attributable to differences in sedimentation rate and surface-sediment organic content. Samples from the oxic layer at Site U1308 lie off the magnetite mixing line (open symbols in Fig. 7c), due to remanent coercivity (H_{cr}) values of ~60 mT, about twice the values below the oxic zone. Following Smirnov and Tarduno (2000), we

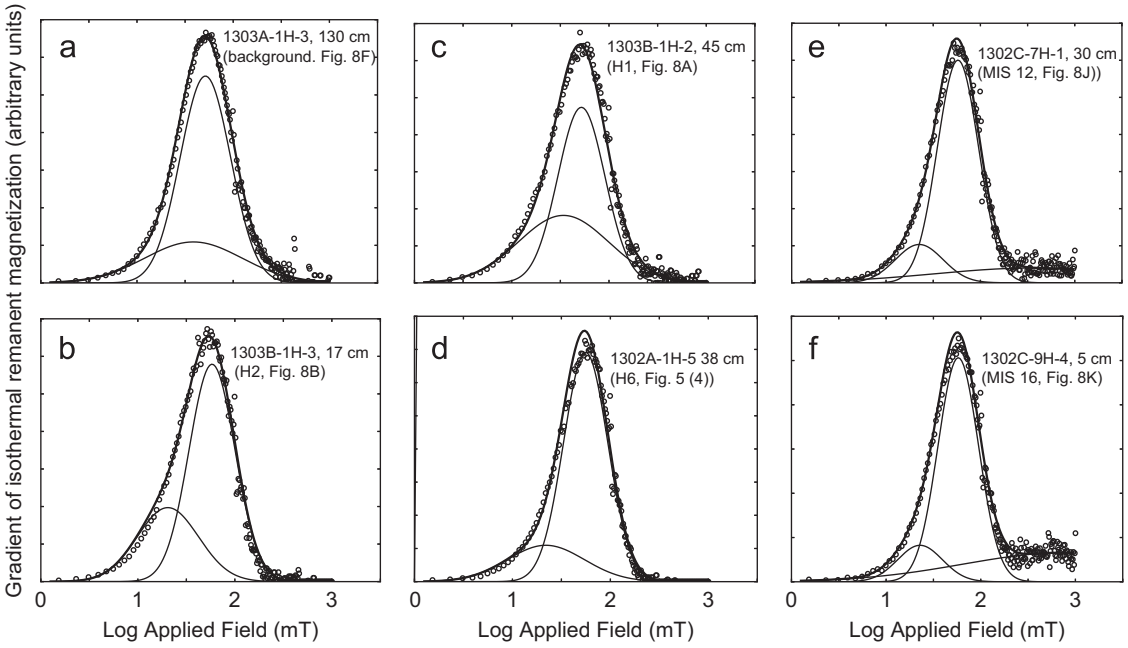

Fig. 9. First derivatives (gradients) of IRM acquisition curves modeled using coercivity spectra. Asymmetry in the gradient curve and prominent low coercivity spectra are associated with ice-rafted debris (IRD) in detrital layers. For Si-rich detrital layers (e)–(f), a third unsaturated higher-coercivity component (associated with hematite) is necessary to model the gradient curves. FORC diagrams for these samples appear in Figs. 5 and 8.

attribute this "offset" from the magnetite mixing line to the presence of maghemite coatings on magnetite grains in the oxic zone that undergo dissolution as the sediment passes through the oxic/anoxic boundary. This is probably a common process affecting magnetite in the oxic zone of pelagic sediments.

Si/Sr and Ca/Si ratios from XRF scanning denote silicate-rich and carbonate-rich detrital layers in which magnetic grain sizes exceed 20 μm, indicating an ice-rafted (IRD) component. The magnetic grain size data confirm that Si/Sr anomalies denote silicate-rich IRD, rather than intervals lacking carbonate. S-ratios and reflectance data indicate that silicate-rich IRD is associated with higher magnetic coercivity due to the presence of hematite, that is apparently not present in calcite-rich IRD. Peaks in Si/Sr and lows in benthic $\delta^{13}C$ are in-step with one another (Fig. 4), indicating that silicate-rich IRD peaks coincide with perturbations of thermohaline circulation affecting bottom waters. Silicate-rich IRD dominates the detrital layer stratigraphy prior to MIS, 16 at least as far back as MIS 42 (~1.3 Ma) at Site U1308 (Fig. 4), whereas calcite-rich IRD became important, especially during late glacial intervals, since MIS 16 and since MIS 18 at Site U1308 and Site U1302/03, respectively. The correspondence of the Site U1302/03 and Site U1308 IRD records (see Channell et al., 2012) implies that both calcite- and silicate-rich IRD are largely supplied from the Laurentide region. The dominant Laurentide silicate-rich IRD was augmented by a Laurentide carbonate-rich source sometime between the onset of the Middle Pleistocene climate transition (MPT) at MIS 22 time (Elderfield et al., 2012) and the base of the section at Site U1302/03 (MIS 18) and the first arrival of icebergs carrying carbonate-rich IRD at distal Site U1308 during MIS 16 (Hodell et al., 2008). The dominance of hematitic IRD prior to the MIS 16 implies a role for either a hematite-bearing (e.g. red sandstone) substrate, or a more oxidized regolith, in supplying IRD, that is partially replaced by a different and/or less weathered source after MIS 16, reminiscent of the "regolith" hypothesis of Clark and Pollard (1998).

Acknowledgments

We thank K. Huang and H. Evans for laboratory assistance. Research supported by National Science Foundation Grants OCE-0850413 and OCE-1014506. Data archives for Site U1308 can be found at http://hurricane.ncdc.noaa.gov/pls/paleox/f?p=519:1:4457963286187086:::P1_STUDY_ID:10250 and http://doi.pangaea.de/10.1594/PANGAEA.808947.

Data archives for Site U1302–03 can be found at http://doi.pangaea.de/10.1594/PANGAEA.808922.

References

Barranco, J., Balsam, W.L., Deaton, B.C., 1989. Quantitative reassessment of brick red lutites: evidence from reflectance spectrophotometry. Mar. Geol. 89, 299–314.

Banerjee, S.K., King, J.W., Marvin, J., 1981. A rapid method for magnetite granulometery with applications to environmental studies. Geophys. Res. Lett. 8, 333–336.

Bond, G., Broecker, W., Johnsen, S., McManus, J., Laberyie, L., Jouzel, J., Bonani, G., 1993. Correlations between climate records from North Atlantic sediments and Greenland ice. Nature 365, 143–147.

Bond, G., Lotti, R., 1995. Iceberg discharges into the North Atlantic on millennial time scales during the last glaciation. Science 267, 1005–1010.

Bond, G., Showers, W., Elliot, M., Evans, M., Lotti, R., Hajdas, I., Bonani, G., Johnson, S., 1999. The North Atlantic's 1-2 kyr climate rhythm: relation to Heinrich Events, Dansgaard/Oeschger cycles and the Little ice Age. In: Webb, et al. (Eds.), Mechanisms of Millennial-Scale Global Climate Change, 112. AGU Geophysical Monograph Series, American Geophysical Union (AGU), Washington, DC, pp. 35–58.

Broecker, W.S., Bond, G., Klas, M., Clark, F., McManus, J., 1992. Origin of the northern Atlantic's Heinrich events. Clim. Dyn. 6, 265–273.

Carter-Stiglitz, B., Moskowitz, B., Jackson, M., 2001. Unmixing magnetic assemblages and the magnetic behavior of bimodal mixtures. J. Geophys. Res. 106, 26397–26411.

Channell, J.E.T., T. Kanamatsu, T. Sato, R. Stein, C.A. Alvarez Zarikian, M.J. Malone, and the Expedition 303/306 Scientists, 2006. North Atlantic Climate, Expeditions 303 and 306 of the riserless drilling platform from St. John's, Newfoundland, to Ponta Delgada, Azores (Portugal), Sites U1302–U1308, 25 September–17 November 2004 and from Ponta Delgada, Azores (Portugal) to Dublin, Ireland, Sites U1312–U1315, 2 March–26 April 2005 Integrated Ocean Drilling Program Management International, Inc. for the Integrated Ocean Drilling Program. Available from: ⟨http://iodp.tamu.edu/publications/exp303_306/30306title.htm⟩.

Channell, J.E.T., Hodell, D.A., Xuan, C., Mazaud, A., Stoner, J.S., 2008. Age calibrated relative paleointensity for the last 1.5 Myr at IODP Site U1308 (North Atlantic). Earth Planet. Sci. Lett. 274, 59–71.

Channell, J.E.T., Hodell, D.A., Romero, O., Hillaire-Marcel, C., de Vernal, A., Stoner, J. S., Mazaud, A., Röhl, U., 2012. A 750-kyr detrital-layer stratigraphy for the North Atlantic (IODP Site U1302-U1303, Orphan Knoll, Labrador Sea). Earth Planet. Sci. Lett. 317–318, 218–230.

Clark, P.U., Pollard, D., 1998. Origin of the middle Pleistocene transition by ice sheet erosion of regolith. Paleoceanography 13, 1–9.
Dankers, P., 1978. Magnetic Properties of Dispersed Natural Iron-Oxides of Known Grain Size. Ph.D. Thesis. University of Utrecht, Utrecht.
Day, R., Fuller, M., Schmidt, V.A., 1977. Hysteresis properties of titanomagnetites: grain-size and compositional dependence. Phys. Earth Planet. Inter. 13, 260–267.
Deaton, B.C., Balsam, W.L., 1991. Visible spectroscopy; a rapid method for determining hematite and goethite concentration in geological materials. J. Sediment. Petrol. 61, 628–632.
Dunlop, D.J., 2002a. Theory and application of the Day plot (M_{rs}/M_s versus H_{cr}/H_c) 1. Theoretical curves and tests using titanomagnetite data. J. Geophys. Res. 107 (B3), 2056, http://dx.doi.org/10.1029/2001JB000486.
Dunlop, D.J., 2002b. Theory and application of the Day plot (M_{rs}/M_s versus H_{cr}/H_c) 2. Application to data for rocks, sediments, and soils. J. Geophys. Res. 107 (B3), 2057, http://dx.doi.org/10.1029/2001JB000487.
Dunlop, D.J., Carter-Stiglitz, B., 2006. Day plots of mixtures of superparamagnetic, single domain, pseudosingle domain, and multidomain magnetites. J. Geophys. Res. 111, B12S09, http://dx.doi.org/10.1029/2006JB004499.
Egli, R., Lowrie, W., 2002. Anhysteretic remanent magnetization of fine magnetic particles. J. Geophys. Res. 107 (B10), 2209, http://dx.doi.org/10.1029/2001JB000671.
Elderfield, H., Ferretti, P., Greaves, M., Crowhurst, S., McCave, I.N., Hodell, D.A., Piotrowski, A.M., 2012. Evolution of ocean temperature and ice volume through the Mid-Pleistocene Climate Transition. Science 337, 704–709.
Elliot, M., Labeyrie, L., Bond, G., Cortijo, E., Turon, J.L., Tisnerat, N., Duplessy, J.C., 1998. Millennial-scale iceberg discharges in the Irminger Basin during the last glacial period: relationship with the Heinrich events and environmental settings. Paleoceanography 13, 433–446.
Expedition 303 Scientists, 2006. Site U1302 and U1303. In: Channell, J.E.T., Kanamatsu, T., Sato, T., Stein, R., Alvarez Zarikian, C.A., Malone, M.J., Expedition 303/306 Scientists. Proceedings of IODP, 303. College Station TX (Integrated Ocean Drilling Program Management International, Inc.), http://dx.doi.org/10.2204/iodp.proc.303306.103.2006, .
Guyodo, Y., Channell, J.E.T., Thomas, R., 2002. Deconvolution of u-channel paleomagnetic data near geomagnetic reversals and short events. Geophys. Res. Lett. 29, 1845, http://dx.doi.org/10.1029/2002GL014963.
Harrison, R.J., Feinberg, J.M., 2008. FORCinel: an improved algorithm for calculating first-order reversal curve distributions using locally weighted regression smoothing. Geochem. Geophys. Geosyst. 9, Q05016, http://dx.doi.org/10.1029/2008GC001987.
Heinrich, H., 1988. Origin and consequences of cyclic ice rafting in the northeast Atlantic Ocean during the past 130,000 years. Quat. Res. 29, 142–152, http://dx.doi.org/10.1016/0033-5894(88)90057-9.
Hemming, S.R., 2004. Heinrich events: massive late Pleistocene detritus layers of the North Atlantic and their global climate imprint. Rev. Geophys. 42, RG1005, http://dx.doi.org/10.1029/2003RG000128.
Heslop, D., Dekkers, M.J., Kruiver, P.P., van Oorschot, I.H.M., 2000. Analysis of isothermal remanent magnetization acquisition curves using the expectation-maximization algorithm. Geophys. J. Int. 148, 58–64.
Hillaire-Marcel, C., de Vernal, A., Bilodeau, G., Wu, G., 1994. Isotope Stratigraphy, sedimentation rates, deep circulation, and carbonate events in the Labrador Sea during the last ~200 ka. Can. J. Earth Sci. 31, 63–89.
Hillaire-Marcel, C., de Vernal, A., McKay, J., 2011. Foraminifer isotope study of the Pleistocene Labrador Sea, northwest North Atlantic (IODP Sites 1302/03 and 1305), with emphasis on paleoceanographical differences between its "inner" and "outer" basins. Mar. Geol. , http://dx.doi.org/10.1016/j.margeo.2010.11.001.
Hiscott, R.N., Aksu, A.E., Mudie, P.J., Parsons, D.F., 2001. A 340,000 year record of ice rafting, paleoclimatic fluctuations, and shelf crossing glacial advances in the southwestern Labrador Sea. Glob. Planet. Change 28, 227–240.
Hodell, D.A., J.E.T, Channell, J.H. Curtis, O.E. Romero and U. Rohl, Onset of "Hudson Strait" Heinrich events in the eastern North Atlantic at the end of the middle Pleistocene transition (~640 ka)? Paleoceanography, 23, PA4218, 10.1029/2008PA001591, 2008.
Hodell, D.A., Curtis, J.H., 2008. Oxygen and carbon isotopes of detrital carbonate in North Atlantic Heinrich events. Mar. Geol. 256, 30–35.
Ji, J., Ge, Y., Balsam, W., Damuth, J.E., Chen, J., 2009. Rapid identification of dolomite using a Fourier Transform Infrared Spectrometer (FTIR): A fast method for identifying Heinrich events in IODP Site U1308. Mar. Geol. 258, 60–68.
King, J.W., Banerjee, S.K., Marvin, J., 1983. A new rock-magnetic approach to selecting sediments for geomagnetic paleointensity studies: application to paleointensity for the last 4000 years. J. Geophys. Res. 88 (1983), 5911–5921.
King, J.W., Channell, J.E.T., 1991. Sedimentary magnetism, environmental magnetism, and magnetistratigraphy. In US National Report to International Union of Geodesy and Geophysics. Rev. Geophys. (Supplement), 358–370.
Kruiver, P.P., Dekkers, M.J., Heslop, D., 2001. Quantification of magnetic coercivity components by the analysis of acquisition curves of isothermal remanent magnetization. Earth Planet. Sci. Lett. 189, 269–276.
Muxworthy, A.R., Roberts, A.P., 2007. First-order reversal curve (FORC) diagrams. In: Gubbins, D., Herrero-Bervera, E. (Eds.), Encyclopedia of Geomagnetism and Paleomagnetism. Springer, Dordrecht, Netherlands, pp. 266–272.
Naafs, B.D.A., Hefter, J., Grützner, J., Stein, R., 2013. Warming of surface waters in the mid-latitude North Atlantic during Heinrich Events. Paleoceanography, 28, http://dx.doi.org/10.1029/2012PA002354.
Pike, C.R., Roberts, A.P., Verosub, K.L., 1999. Characterizing interactions in fine magnetic particle systems using first order reversal curves. J. Appl. Phys. 85, 6660–6667, http://dx.doi.org/10.1063/1.370176.
Rashid, H., Hesse, R., Piper, D.J.W., 2003. Evidence for an additional Heinrich event between H5 and H6 in the Labrador Sea. Paleoceanography 18 (4), 1077, http://dx.doi.org/10.1029/2003PA000913.
Rasmussen, T.L., Oppo, D.W., Thomsen, E., Lehman, S.J., 2003. Deep sea records from the southeast Labrador Sea: ocean circulation changes and ice-rafting events during the last 160,000 years. Paleoceanography 18 (1), 1018, http://dx.doi.org/10.1029/2001PA000736.
Roberts, A.P., Pike, C.R., Verosub, K.L., 2000. First-order reversal curve diagrams: a new tool for characterizing the magnetic properties of natural samples. J. Geophys. Res. 105, 28461–28475, http://dx.doi.org/10.1029/2000JB900326.
Robertson, D.J., France, D.E., 1994. Discrimination of remanence-carrying minerals in mixtures, using isothermal remanent magnetization acquisition curves. Phys. Earth Planet. Inter. 84, 223–234.
Robinson, S.G., Maslin, M.A., McCave, I.N., 1995. Magnetic susceptibility variations in Upper Pleistocene deep-sea sediments of the NE Atlantic: implications for ice rafting and paleocirculation at the last glacial maximum. Paleoceanography 10, 221–250.
Smirnov, A.V., Tarduno, J.A., 2000. Low-temperature magnetic properties of pelagic sediments (Ocean Drilling Program Site 805C): Tracers of maghemitization and magnetic mineral reduction. J. Geophys. Res. 105 (B7), 16457–16471.
Stoner, J.S., Channell, J.E.T., Hillaire-Marcel, C., 1995. Late Pleistocene relative geomagnetic paleointensity from the deep Labrador Sea: regional and global correlations. Earth Planet. Sci. Lett. 134, 237–252.
Stoner, J.S., Channell, J.E.T., Hillaire-Marcel, C., 1996. The magnetic signature of rapidly deposited detrital layers from the deep Labrador Sea: relationship to North Atlantic Heinrich layers. Paleoceanography 11, 309–325.
Stoner, J.S., Channell, J.E.T., Hillaire-Marcel, C., 1998. A 200 kyr geomagnetic chronostratigraphy for the Labrador Sea: indirect correlation of the sediment record to SPECMAP. Earth Planet. Sci. Lett. 159, 165–181.
Stoner, J.S., Channell, J.E.T., Hillaire-Marcel, C., Kissel, C., 2000. Geomagnetic paleointensity and environmental record from Labrador Sea Core MD95-2024: Global marine sediment and ice core chronostratigraphy for the last 110 kyr. Earth Planet Sci. Lett. 183, 161–177.
Thomas, R., Guyodo, Y., Channell, J.E.T., 2003. U-channel track for susceptibility measurements. Geochem. Geophys. Geosyst. (G^3) 1050, http://dx.doi.org/10.1029/2002GC000454.
Van Kreveld, S.A., Knappertsbusch, M., Ottens, J., Ganssen, G., van Hinte, J., 1996. Biogenic carbonate and ice-rafted debris (Heinrich layer) accumulation in deep-sea sediments from a Northeast Atlantic piston core. Mar. Geol. 131, 21–46.
Weeks, R., Laj, C., Endignoux, L., Fuller, M., Roberts, A., Manganne, R., Blanchard, E., Goree, W., 1993. Improvements in long-core measurement techniques: applications in palaeomagnetism and palaeoceanography. Geophys. J. Int. 114, 651–662.